Erschienen in: Nature Materials ; 18 (2019), 10. - S. 1118-1123
https://dx.doi.org/10.1038/s41563-019-0446-9

Active particles sense micromechanical properties of glasses

Celia Lozano[1], Juan Ruben Gomez-Solano[1,2] and Clemens Bechinger[1*]

Understanding the mechanical properties of glasses is a great scientific challenge. A powerful technique to study the material response on a microscopic scale is microrheology, in which one analyses the translational dynamics of an externally driven probe particle. Here we show that the translational and rotational dynamics of a self-propelled probe particle with an unconstrained orientational motion can be used to gather information about the mechanical properties of a colloidal glassy system. We find that its rotational diffusion coefficient continuously increases towards the glass transition and drops down in the glassy state. Such unexpected behaviour demonstrates a strong coupling mechanism between the orientation of the active probe particle and the glassy structure, which can be well described by a simple rheological model. Our results suggest that active probe particles may be useful for the micromechanical characterization of complex materials.

A universal property of glasses is that they continuously change from a liquid into an amorphous solid, for example, on cooling or increasing the particle density[1–4]. Although their global structure hardly changes on approaching the glass transition, material properties, such as viscosity, inverse self-diffusivity and the relaxation time, increase or even diverge[3,5]. Such behaviour is accompanied by cooperative particle rearrangements[2,6,7], which lead to an intermittent dynamics that affects, for example, the free volume[8], local yield stress[9], localization of defects[10] and local thermal energy[11] of the particles. At microscopic scales, structural information can be obtained by active microrheology in which a single probe particle is driven by an external force through the medium under investigation at either a constant force or velocity[12,13]. Owing to the strong coupling between the driven probe particle and its environment, this allows us to obtain detailed information on the local mechanical and transport properties of glasses[14–16]. However, previous studies with spherical probes only considered their translational motion[17,18]. Here we demonstrate that structural information on glasses can also be inferred by evaluating the orientational dynamics of a probe particle. Contrary to externally driven probes, which are forced along a given direction, here we employ an active, that is self-propelled, probe particle (APP) whose orientation fluctuates over time[19]. We demonstrate that, in addition to its translational motion, the orientational dynamics of an APP strongly couples to the slow relaxation of the disordered surroundings, which leads to a maximum of the rotational diffusion coefficient at the glass transition where the relaxation time becomes largest. Our results are supported by a simple viscoelastic mechanical model and suggest that APPs may be valuable tools for the mechanical characterization of amorphous materials.

Our experiments were performed in a two-dimensional (2D) cell that contained a 50:50 binary mixture of colloidal particles with diameters of 4.4 and 6.3 μm suspended in a water–lutidine mixture which was kept 8 °C below its lower critical temperature, $T_c = 34$ °C (ref. [20]). Under such conditions, the particles perform a diffusive Brownian motion. Their interactions are dominated by steric interactions due to the small Debye screening length (~12 nm (ref. [20])), which leads to a rather short-ranged electrostatic repulsion. The crystallization of the colloidal mixture is suppressed over the entire range of the area fractions $0 < \varphi < 0.845$ considered in this work, and a glassy state forms above $\varphi_g \geq 0.776$, as confirmed by the mean square displacement, the self-intermediate scattering function and the non-Gaussian parameter (Methods and Supplementary Fig. 1). We added a very small amount ($\varphi < 0.01$) of Janus particles (APPs) with a $\sigma = 6.3$ μm diameter. On laser illumination, APPs self-propel opposite to their cap with their propulsion velocity v_0 controlled by the light intensity[21]. For an isolated APP ($\varphi = 0$), its rotational dynamics is entirely diffusive and, in particular, does not change in the presence of propulsion[22]. Owing to interactions with its surrounding particles, the APP's velocity v slows down with increasing φ (Methods and Supplementary Fig. 2b). As a φ-independent quantifier of the APP propulsion, in the following we use $v_0 = v(\varphi = 0)$. As shown further below, the propulsion was chosen to be sufficiently low to avoid a shift of the glass transition of the colloidal background. Owing to hydrodynamic interactions with the walls, in addition to the translational dynamics, the rotational motion of APPs is also confined to 2D[21] (Methods gives further details).

Figure 1a shows a trajectory of a passive ($v_0 = 0\,\mu m\,s^{-1}$) Janus particle in a dense colloidal background with $\varphi = 0.730$, that is, below φ_g, over 500 s. As expected, it remains rather localized due to confinement by its neighbours and undergoes only minimal positional and orientational changes. In contrast, when the Janus particle is made active ($v_0 = 1.0\,\mu m\,s^{-1}$), a strongly enhanced translational motion is observed (Fig. 1b). Interestingly, when the area fraction is increased to $\varphi_g = 0.776$, the translational motion does not slow down (Fig. 1c). Only above the glass transition does the motion of the APP qualitatively change to perform an arrested motion (caging) and rare events of cage hopping (Fig. 1d). Such φ-dependent dynamics, which is qualitatively identical to the well-known arrested behaviour of passive particles in a colloidal glass[1,3,4], is here demonstrated for an active particle. To understand how the motion of the APP is affected by its surroundings, we calculated their corresponding translational mean squared displacement $\langle \Delta r(t)^2 \rangle = \langle [r(t+t_0) - r(t_0)]^2 \rangle t_0$. The results for $v_0 = 1.0\,\mu m\,s^{-1}$ are shown in Fig. 1e for different area fractions. For $\varphi = 0$, the translational dynamics of an APP shows the expected short-time ballistic directed motion, whereas at

[1]Fachbereich Physik, Universität Konstanz, Konstanz, Germany. [2]Present address: Instituto de Fisica, Universidad Nacional Autonoma de Mexico, Mexico City, Mexico. *e-mail: clemens.bechinger@uni-konstanz.de

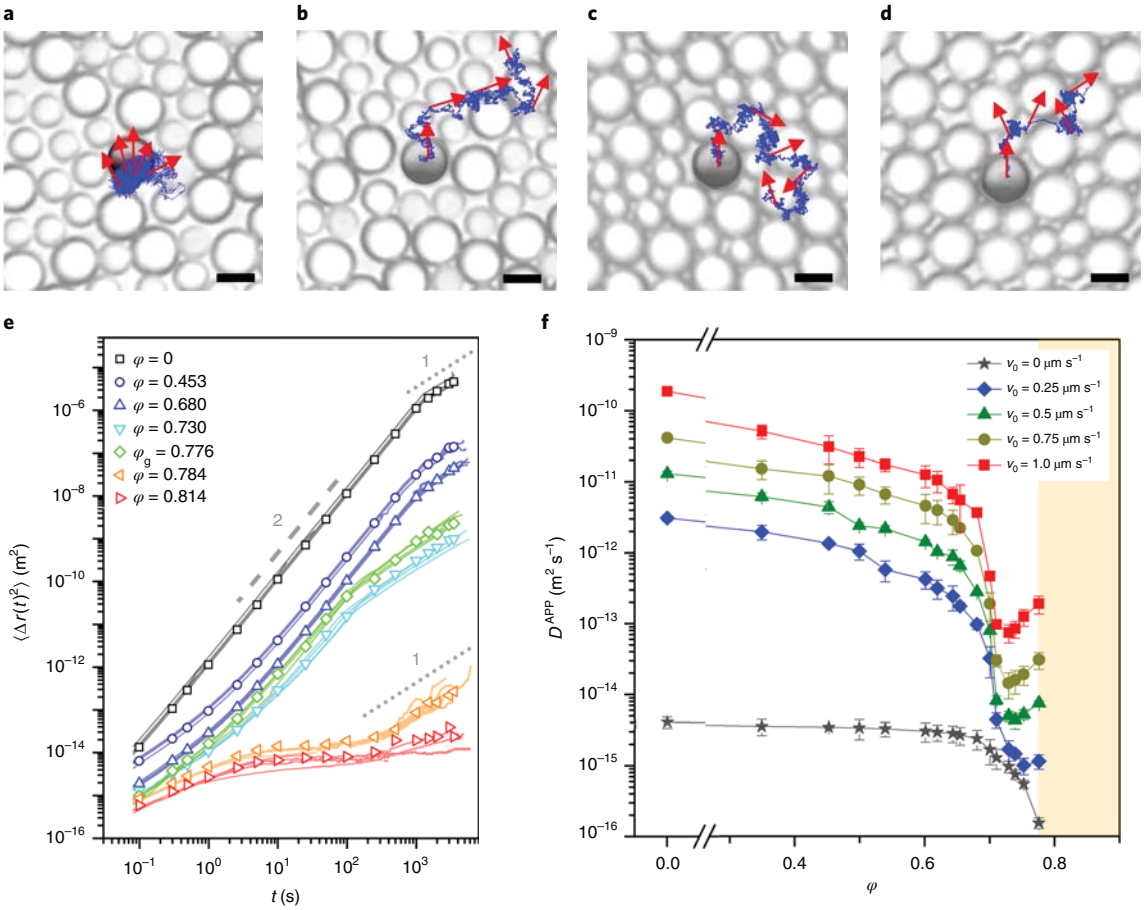

Fig. 1 | APP dynamics within a dense binary colloidal suspension. a–d, Trajectories over 500 s with positions and orientations indicated as blue lines and red arrows for $\varphi = 0.730$, $v_0 = 0\,\mu m\,s^{-1}$ (**a**), $\varphi = 0.730$, $v_0 = 1.0\,\mu m\,s^{-1}$ (**b**), $\varphi_g = 0.776$, $v_0 = 1.0\,\mu m\,s^{-1}$ (**c**) and $\varphi = 0.784$, $v_0 = 1.0\,\mu m\,s^{-1}$ (**d**). Scale bar, 5 μm. **e**, Translational mean-squared displacement $\langle \Delta r(t)^2 \rangle$ with $v_0 = 1.0\,\mu m\,s^{-1}$ for different φ. The lines correspond to independent measurements and symbols represent their average. **f**, Effective diffusion D^{APP} for different propulsion velocities v_0. The orange shading indicates the glass region.

long times the orientational changes lead to a diffusive behaviour. For $0.453 \leq \varphi \leq \varphi_g$ the short-time behaviour becomes increasingly affected by collisions with the colloidal background, which leads to a superdiffusive short-time APP dynamics, as seen by the slope in the mean squared displacement, which is larger than one but below two (Fig. 1e). For $\varphi > \varphi_g$, a plateau-like subdiffusive regime is observed. We emphasize that the value of $\varphi_g = 0.776$, where this distinguished feature occurs, is identical to the glass transition of the binary mixture inferred from a passive probe measurement (Methods and Supplementary Fig. 1). This confirms that for the propulsion velocities considered here, the glass transition is not disturbed by the APP. Independent of the area fraction and, in agreement with passive glasses, the long-time behaviour of the APPs remains always diffusive. For $\varphi < \varphi_g$, the φ-dependent effective diffusion coefficient $D^{APP} = \langle \Delta r(t)^2 \rangle / 4t$, is shown in Fig. 1f. Contrary to passive particles, whose diffusion coefficient monotonically decreases with increasing φ (stars in Fig. 1f), D^{APP} exhibits a minimum just below φ_g and increases afterward.

To understand this behaviour in more detail, we studied the rotational dynamics of APPs. Figure 2a shows the corresponding angular mean square displacements $\langle \Delta\theta(t)^2 \rangle = [\theta(t+t_0) - \theta(t_0)]^2 \rangle$ t_0 for $v_0 = 1.0\,\mu m\,s^{-1}$ and different area fractions. The APP orientation $\theta(t)$ was obtained from the optical contrast due to the carbon cap (Fig. 1a–d and Methods). Independent of φ, $\langle \Delta\theta(t)^2 \rangle$ linearly increases in time, that is, $\langle \Delta\theta(t)^2 \rangle = 2D_\theta^{APP} t$ where D_θ^{APP} is the orientational diffusion coefficient. Contrary to a passive probe whose rotational diffusion coefficient $D_\theta = 0.0011 \pm 5 \times 10^{-5}\,s^{-1}$ is unaffected by the area fraction (Fig. 2b), D_θ^{APP} strongly depends on φ (Fig. 2c). Remarkably, D_θ^{APP} (φ) shows a pronounced maximum right at the glass transition. Although the peak amplitude depends on v_0 (Fig. 2c inset), the location of the peak is always at φ_g. Note that the onset of the enhancement of D_θ^{APP} coincides with the minimum of D^{APP} (Fig. 1f). This suggests a strong coupling between the orientational and the translational motion close to the glass transition. Such behaviour, which has not been reported in previous studies[23,24], is in agreement with the observed φ-dependent correlation between angular and translational displacements of the APP (Fig. 2d–g). We emphasize that a peak of D_θ^{APP} at φ_g also appears for slightly different diameters of the colloids that comprise the binary suspension ($\sigma = 1.8\,\mu m$ and $2.2\,\mu m$), and thus suggests the maximum of the rotational diffusion coefficient at the glass transition to be a generic feature (Methods and Supplementary Fig. 3). Notably, the rotational diffusion time $(1/D_\theta^{APP})$ of the APP becomes fastest and remains finite at φ_g. This is in contrast to many other quantities that typically increase and even diverge on approaching the glass transition[1,3,5,25].

For a qualitative understanding of the enhanced rotational diffusion of a spherical APP, we recall the relationship between the propulsion velocity of an active particle and the velocity field of the surrounding fluid[26] $\mathbf{v}(t) = \mathbf{w}_\Sigma(t) - \mathbf{w}_{slip}(t)$. Here $\mathbf{v}(t) = v\mathbf{u}(t)$ is the particle propulsion velocity and $\mathbf{u}(t)$ corresponds to its orientation, $\mathbf{w}_\Sigma$ is the velocity outside the region perturbed by the propulsion mechanism and $\mathbf{w}_{slip}(t)$ is the fluid's slip velocity near the particle

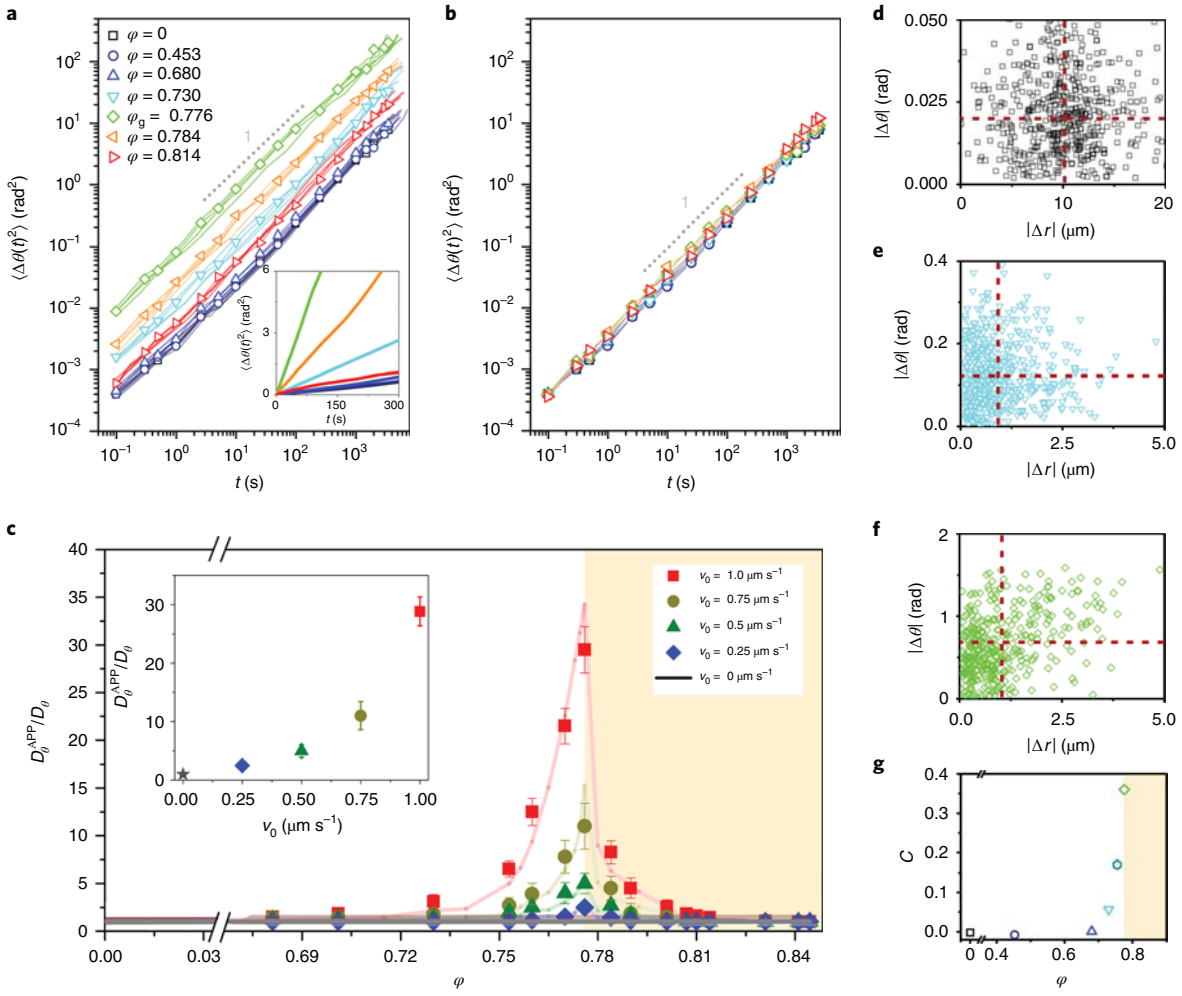

Fig. 2 | Rotational APP dynamics. a, The orientational mean square displacement $\langle \Delta\theta(t)^2 \rangle$ of an active particle with $v_0 = 1.0\,\mu m\,s^{-1}$ within a binary colloidal suspension with different area fraction φ. Lines correspond to $\langle \Delta\theta(t)^2 \rangle$ obtained from four independent measurements and symbols represent their average. Inset: linear–linear representation of the main figure. **b**, Corresponding $\langle \Delta\theta(t)^2 \rangle$ of a passive Janus particle ($v_0 = 0\,\mu m\,s^{-1}$). **c**, Normalized APP rotational diffusion coefficient versus the area fraction of the binary colloidal background for different self-propulsion velocities. Experimental data (averaged over 4–10 particles) and numerical solutions of equation (5) are shown as symbols and lines, respectively. The error bars represent the s.d. Inset: experimentally observed enhanced rotational dynamics of APP versus particle propulsion at $\varphi_g = 0.776$. **d**–**f**, Scatter plots of translational $|\Delta r|$ and orientational $|\Delta\theta|$ displacements within $\Delta t = 10$ s and for $v_0 = 1.0\,\mu m\,s^{-1}$ for $\varphi = 0$ (**d**), $\varphi = 0.73$ (**e**) and $\varphi_g = 0.776$ (**f**). The horizontal and vertical dashed lines indicate the mean value of the corresponding displacements. **g**, Correlation coefficient C, calculated from $C = (\sum_{i=1}^{n} (\Delta r_i - \overline{\Delta r})(\Delta\theta_i - \overline{\Delta\theta}))/(\sqrt{\sum_{i=1}^{n} (\Delta r_i - \overline{\Delta r})^2 \sum_{i=1}^{n} (\Delta\theta_i - \overline{\Delta\theta})^2})$ where Δr_i is the translational displacement in step i, and $\Delta\theta_i$ the rotational displacement in step i, as a function of φ. The expressions with the overlines are the corresponding mean values. The orange dashed box indicates the glass region.

surface. The latter is created by the conversion of energy (optical, chemical and thermal) from the surroundings into a surface fluid flow. In a quiescent fluid, this leads to $\mathbf{v}(t) = -\mathbf{w}_{slip}(t)$, that is, the particle's motion is opposite to the slip flow (and thus fulfils force-free conditions). In addition, the particle orientation is parallel to its direction of motion $\dot{\mathbf{r}}(t)$. This quiescent fluid approximation (in the absence of external pressure gradients) is no longer justified in (glassy) viscoelastic media, whose relaxation times are longer than or comparable with the timescale of the active particle motion (Supplementary Fig. 4a). Then, the APP interacts with its own time-delayed perturbation field and $\mathbf{w}_\Sigma(t) \neq 0$. According to the above equation, this will affect $\mathbf{v}$. As the APP has a finite size and $\mathbf{w}_\Sigma$ varies in space and time, the APP propulsion direction (and thus its orientation) may no longer be parallel to its orientation but become misaligned (Fig. 3a–e). As a consequence, a time-dependent stochastic torque with zero mean acts on the particle, which leads to an increased orientational motion and so to the enhancement of D_θ^{APP} (Supplementary Fig. 5).

To visualize directly the mechanical coupling of the APP orientation to the colloidal background, exemplarily we discuss the situation for $\varphi = 0.825$ in which no cage hopping occurs on our experimental timescales. As the mechanical coupling to the APP increases with an increasing size ratio of the APP and the background particles[12], we performed these experiments using slightly smaller colloids ($\sigma = 1.7$ and 2.4 μm). Note that, under such conditions, the enhancement of D_θ^{APP} is about a factor of eight (Supplementary Fig. 3). As seen in Fig. 3f, the angular motion of the APP is highly correlated with the circular motion of the particles next to the APP. Quantitative information about the mechanical coupling is obtained from the time correlation between the APP's orientation and the mean cage orientation $\theta_{cage} = \frac{1}{N}\sum_{i=1}^{N} \theta_i$, with N the number of particles that form the cage and θ_i their angle relative to a reference axis (Fig. 3f inset).

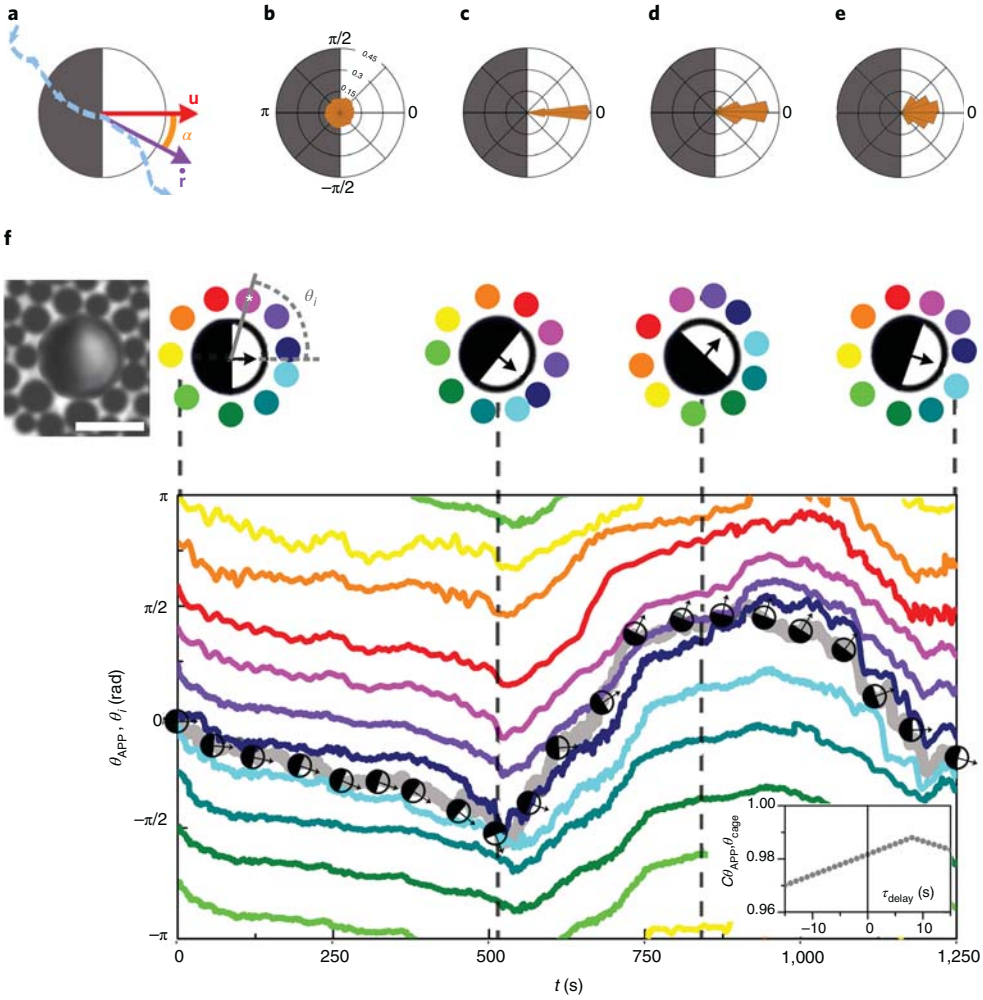

Fig. 3 | Mechanical coupling between APP and next neighbours. a, Sketch of an APP with a propulsion direction $\dot{\mathbf{r}}$ together with its current cap orientation u and the enclosed angle α. The dashed line schematically shows the APP's trajectory. **b**–**e**, Probability distribution of the angle α for a time interval of 0.5 s for $\varphi = 0$, $v_0 = 0\,\mu m\,s^{-1}$ (**b**), $\varphi = 0$, $v_0 = 1.0\,\mu m\,s^{-1}$ (**c**), $\varphi = 0.730$, $v_0 = 1.0\,\mu m\,s^{-1}$ (**d**), $\varphi = 0.776$, $v_0 = 1.0\,\mu m\,s^{-1}$ (**e**). **f**, Experimental snapshot of an APP immersed in a binary colloidal suspension ($\varphi = 0.825$, $\sigma = 1.7$ and 2.4 μm). Scale bar, 5 μm. Temporal evolution of the orientation of the APP and the cage particles, the latter coloured to facilitate positional changes. The angle θ_i denotes the bond-angle location of particle i relative to the horizontal reference axis. Time dependence of the angular particle positions (colour code corresponding to the top figure) for $v_0 = 1.0\,\mu m\,s^{-1}$ (bottom). The grey line shows the temporal evolution of the orientation of the Janus particle θ_{APP}. Inset: corresponding normalized cross-correlation of the angular motion of the APP and the cage, $c\theta_{APP,\theta_{cage}}(\tau_{delay}) = \sum_{t=-\infty}^{\infty}[\theta_{APP}(t-\tau_{delay})\theta_{cage}(t)]$, where τ_{delay} corresponds to the time delay between θ_{APP} and θ_{cage}.

We find that the APP orientation lags behind the cage orientation for several seconds, which is in agreement the time-delayed mechanical response to the surrounding medium.

In the following, we study a minimal model, which describes the mechanical response of an APP in a glassy environment (a more general discussion is given in Methods). We start by considering the motion of an isolated APP ($\varphi = 0$), that is, in a purely viscous fluid. A Newtonian fluid is modelled by a dashpot (characterized by the solvent's viscosity η_∞), which leads to a viscous damping of an APP propelling with velocity $\mathbf{v}(t) = v\mathbf{u}(t)$ where $\mathbf{u} = (\cos\theta, \sin\theta)$ is the instantaneous particle orientation[21] (Fig. 4a). As a result of the instantaneous (compared to the APP dynamics) relaxation of the molecular fluid, the viscous damping element always points opposite to $\mathbf{u}$. This is no longer true at higher area fractions when the colloidal background becomes viscoelastic with a time-delayed response[27,28] (Fig. 3). When an APP moves with velocity $\dot{\mathbf{r}}$ through a viscoelastic medium, it experiences a drag force:

$$\mathbf{F}_{drag}(t) = -\int_{-\infty}^{t} \Gamma(t-t')\,\dot{\mathbf{r}}(t')\,dt' \qquad (1)$$

where the coupling between the APPs motion and the surrounding is considered by the memory kernel $\Gamma(t) = 3\pi\sigma G_\varphi(t)$ with G_φ being the corresponding stress-relaxation modulus. In the absence of inertial effects, the total force exerted on the APP at time t is given by the non-Markovian Langevin equation $\mathbf{F}_{drag}(t) + \boldsymbol{\xi}(t) + \mathbf{F}_{prop}(t) = 0$, where $\boldsymbol{\xi}(t)$ is a noise term with zero mean, which mimics the fluctuating force exerted by the environment (Methods). Note that the total hydrodynamic force exerted by the medium on the particle vanishes on average, $<\mathbf{F}_{drag}(t) + \mathbf{F}_{prop}(t)> = -<\boldsymbol{\xi}(t)> = 0$, and thereby fulfils the force-free condition. The term $\mathbf{F}_{prop}(t)$ is an internal force[29] that describes the propulsion of the APP with velocity $\mathbf{v}$:

$$\mathbf{F}_{prop}(t) = -v\int_{-\infty}^{t} \Gamma(t-t')\,\mathbf{u}(t')\,dt' \qquad (2)$$

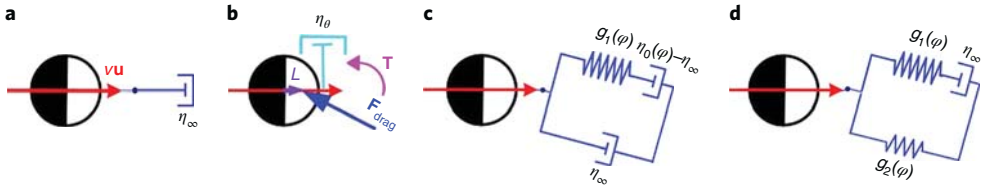

Fig. 4 | Mechanical model of an APP within a viscoelastic environment. a, Schematic representation of the viscous (dashpot) coupling of a spherical active particle moving at propulsion velocity $v\mathbf{u}$ in a purely viscous liquid. **b**, Corresponding model for the APP's orientation with a dashpot with η_θ, which mimics the viscous response of the fluid, and a force $\mathbf{F}_{drag}$ that acts on the APP with a lever arm L, which models the delayed mechanical response of the surrounding fluid relative to the particle orientation both below and above φ_g. **T** represents the effective internal torque due to the delayed response of the fluid. **c**, Corresponding coupling between an APP and a three-element viscoelastic-fluid Jeffreys liquid model (two dashpots with viscosities η_∞ and $\eta_0(\varphi)-\eta_\infty$ (where $\eta_0(\varphi)$ is the zero-shear viscosity) and an elastic spring with stiffness $g_1(\varphi)$, which mimics the rheological response of the surrounding colloidal suspension below φ_g. **d**, Translational coupling between an APP with a three-element viscoelastic-solid SLS model (two springs with stiffness $g_1(\varphi)$ and $g_2(\varphi)$, and a dashpot with viscosity η_∞), which mimics the mechanical response of the surrounding colloidal suspension above φ_g.

Owing to the memory kernel in the response of the viscoelastic background, the drag force is:

$$\mathbf{F}_{drag}(t) = -\nu \int_{-\infty}^{t} \Gamma(t-t')\,\mathbf{u}(t')\,dt' - \boldsymbol{\xi}(t) \tag{3}$$

Importantly, apart from small deviations due to noise, the drag force $\mathbf{F}_{drag}(t)$ is antiparallel to $\mathbf{F}_{prop}(t)$, but misaligned relative to the particle orientation $\mathbf{u}(t)$, the latter depending on all previous times. As a result, the APP is subjected to a time-dependent torque:

$$\mathbf{T}(t) = \mu\sigma\,\mathbf{u}(t) \times \mathbf{F}_{drag}(t) \tag{4}$$

where we have introduced an effective lever arm $L = \mu\sigma\mathbf{u}(t)$, which is defined relative to the particle centre (Fig. 4b). As the size of L depends on the local structure, it is considered as a free fitting parameter μ. Accordingly, the 2D orientational motion of an APP can be modelled by the following Markovian Langevin equation:

$$\pi\sigma^3\eta_\theta\dot{\theta}(t) + \xi_\theta(t) + T(t) = 0 \tag{5}$$

where η_θ is the rotational viscosity (extracted from the slope of the $\langle\Delta\theta(t)^2\rangle$), $\eta_\theta = k_B T(t)/(\pi\sigma^3 D_\theta)$ (Fig. 2b), which is memory independent and $T(t)$ is the modulus of the torque. Here, $\boldsymbol{\xi}_\theta(t)$ is a Gaussian noise of zero mean and $\xi_\theta(t)\xi_\theta(t') = 2k_B T\pi\sigma^3\eta_\theta\delta(t-t')$, which mimics thermal fluctuations. In combination with the noise, the presence of a time-dependent torque leads to an enhanced rotational diffusion coefficient as observed in our experiments.

To numerically solve equation (5), one needs an explicit expression of the mechanical response functions of the surrounding medium. Below φ_g, it has been demonstrated that the viscoelastic colloidal environment can be described by a Jeffreys model[27,28] with the stress-relaxation modulus (Fig. 4c).

$$G_{\varphi<\varphi_g}(t) = 2\eta_\infty\delta(t) + \frac{\eta_0(\varphi)-\eta_\infty}{\tau(\varphi)} e^{-\frac{t}{\tau(\varphi)}} \tag{6}$$

The first and second terms characterize the (on the timescale of the APP) instantaneous relaxation of the molecular solvent with viscosity η_∞ and the time-delayed response of the strained colloidal suspension, respectively. The latter process is described by the stress-relaxation time $\tau(\varphi) = \frac{\eta_0(\varphi)-\eta_\infty}{g_1(\varphi)}$ with viscosity $\eta_0(\varphi)$ and the elastic modulus $g_1(\varphi)$, both of which depend on the colloidal area fraction. Above φ_g, the mechanical properties of the colloidal suspension change from a liquid- to a solid-like behaviour and the motion of the APP becomes strongly arrested[3]. Neglecting the sporadic cage-hopping events, the mechanical properties of a glassy system have been demonstrated to be in accordance with a standard linear solid[30] (SLS) model (Fig. 4d). The stress-relaxation modulus of the SLS is given by

$$G_{\varphi>\varphi_g}(t) = g_2(\varphi) + g_1(\varphi) e^{-\frac{t}{\tau_{SLS}(\varphi)}} \tag{7}$$

The first term accounts for the stiffness due to the local confinement $g_2(\varphi)$, which leads to a dynamical arrest over the experimental timescales, whereas the second term captures the elastic cage deformation with a stress relaxation time $\tau_{SLS}(\varphi)$ (Methods gives further details).

With this approach, we were able to numerically solve equation (5) and obtain two independent solutions for the rotational diffusion D_θ^{APP} of the APP, below and above the glass transition. The results are plotted as solid lines in Fig. 2c. As the only fitting parameter, we adjusted the value of the parameter μ, which describes the effective lever arm. For simplicity, we assumed that μ is a constant in each regime. With the additional constraint that the solutions of both rheological models coincide at φ_g, the best agreement with our experimental data was obtained for $\mu = 0.13$ for $\varphi < \varphi_g$ and $\mu = 0.50$ for $\varphi > \varphi_g$, respectively. Despite some deviations of this simple micromechanical description, in particular near φ_g, we found an excellent overall agreement with our experimental data. As the dynamical properties of glasses are more complex than the mere rheological response of the Jeffreys and SLS models, the good agreement with our experimental data suggests that, for example, dynamical and spatial heterogeneities have no central role for the orientational response of an APP within a glassy structure. Instead, the time-delayed response of the APP due to the viscoelasticity of the environment is sufficient to understand the enhancement of its rotational dynamics near φ_g. We expect, however, that this will not apply to the translational and long-time dynamics of APPs in glassy environments where the material's heterogeneities should become important.

Finally, we remark that, contrary to many other materials' properties, which diverge on approaching the glass transition[1,3,5,10,24], the fastened rotational diffusion avoids strongly increasing measuring timescales typically required when approaching the glass transition. The strong orientational response of light-activated APPs within dense and slowly relaxing colloidal suspensions is the result of the time-delayed mechanical response of their surroundings and should equally occur for other APP-driving mechanisms[19,31,32] and a large variety of materials[27,33]. Therefore, active particles might be useful mechanical microprobes to study the properties of soft materials such as (bio)polymers, worm-like micelles and cellular tissues[34]. Our results are also relevant for numerical studies of active glasses[35,36] and mixtures of active and passive particles[37,38], which so far have not considered the enhancement of particle orientation

dynamics. Moreover, given that the natural environment of living microswimmers is often viscoelastic[39–41], our findings about the dynamics of active particles in such systems may be useful for designing navigation strategies of microorganisms under realistic conditions.

References

1. Berthier, L. & Biroli, G. Theoretical perspective on the glass transition and amorphous materials. *Rev. Mod. Phys.* **83**, 587–645 (2011).
2. Berthier, L., Biroli, G., Bouchaud, J.-P., Cipelletti, L. & van Saarloos, W. *Dynamical Heterogeneities in Glasses, Colloids, and Granular Media* (Oxford Univ. Press, 2011).
3. Hunter, G. L. & Weeks, E. R. The physics of the colloidal glass transition. *Rep. Prog. Phys.* **75**, 066501 (2012).
4. Pusey, P. N. & van Megen, W. Phase behaviour of concentrated suspensions of nearly hard colloidal spheres. *Nature* **320**, 340–342 (1986).
5. Brambilla, G. et al. Probing the equilibrium dynamics of colloidal hard spheres above the mode-coupling glass transition. *Phys. Rev. Lett.* **102**, 085703 (2009).
6. Stevenson, J. D., Schmalian, J. & Wolynes, P. G. The shapes of cooperatively rearranging regions in glass-forming liquids. *Nat. Phys.* **2**, 268–274 (2006).
7. Candelier, R. et al. Spatiotemporal hierarchy of relaxation events, dynamical heterogeneities, and structural reorganization in a supercooled liquid. *Phys. Rev. Lett.* **105**, 135702 (2010).
8. Spaepen, F. Homogeneous flow of metallic glasses: a free volume perspective. *Scr. Mater.* **54**, 363–367 (2006).
9. Cubuk, E. D. et al. Structure–property relationships from universal signatures of plasticity in disordered solids. *Science* **358**, 1033–1037 (2017).
10. Gokhale, S., Hima Nagamanasa, K., Ganapathy, R. & Sood, A. K. Growing dynamical facilitation on approaching the random pinning colloidal glass transition. *Nat. Commun.* **5**, 4685 (2014).
11. Zylberg, J., Lerner, E., Bar-Sinai, Y. & Bouchbinder, E. Local thermal energy as a structural indicator in glasses. *Proc. Natl Acad. Sci. USA* **114**, 7289–7294 (2017).
12. Squires, T. M. & Brady, J. F. A simple paradigm for active and nonlinear microrheology. *Phys. Fluids* **17**, 073101 (2005).
13. Shore, K. A. & Alan Shore, K. Microrheology, by E. M. Furst and T. M. Squires. *Contemp. Phys.* **59**, 222–223 (2018).
14. Habdas, P., Schaar, D., Levitt, A. C. & Weeks, E. R. Forced motion of a probe particle near the colloidal glass transition. *Europhys. Lett.* **67**, 477–483 (2004).
15. Winter, D., Horbach, J., Virnau, P. & Binder, K. Active nonlinear microrheology in a glass-forming Yukawa fluid. *Phys. Rev. Lett.* **108**, 028303 (2012).
16. Wilson, L. G., Harrison, A. W., Poon, W. C. K. & Puertas, A. M. Microrheology and the fluctuation theorem in dense colloids. *Europhys. Lett.* **93**, 58007 (2011).
17. Gruber, M., Abade, G. C., Puertas, A. M. & Fuchs, M. Active microrheology in a colloidal glass. *Phys. Rev. E* **94**, 042602 (2016).
18. Puertas, A. M. & Voigtmann, T. Microrheology of colloidal systems. *J. Phys. Condens. Matter* **26**, 243101 (2014).
19. Bechinger, C. et al. Active particles in complex and crowded environments. *Rev. Mod. Phys.* **88**, 045006 (2016).
20. Hertlein, C., Helden, L., Gambassi, A., Dietrich, S. & Bechinger, C. Direct measurement of critical Casimir forces. *Nature* **451**, 172–175 (2008).
21. Gomez-Solano, J. R. et al. Tuning the motility and directionality of self-propelled colloids. *Sci. Rep.* **7**, 14891 (2017).
22. Buttinoni, I., Volpe, G., Kümmel, F., Volpe, G. & Bechinger, C. Active Brownian motion tunable by light. *J. Phys. Condens. Matter* **24**, 284129 (2012).
23. Edmond, K. V., Elsesser, M. T., Hunter, G. L., Pine, D. J. & Weeks, E. R. Decoupling of rotational and translational diffusion in supercooled colloidal fluids. *Proc. Natl Acad. Sci. USA* **109**, 17891–17896 (2012).
24. Debenedetti, P. G. & Stillinger, F. H. Supercooled liquids and the glass transition. *Nature* **410**, 259–267 (2001).
25. van Megen, W., Mortensen, T. C., Williams, S. R. & Müller, J. Measurement of the self-intermediate scattering function of suspensions of hard spherical particles near the glass transition. *Phys. Rev. E* **58**, 6073–6085 (1998).
26. Brady, J. F. Particle motion driven by solute gradients with application to autonomous motion: continuum and colloidal perspectives. *J. Fluid Mech.* **667**, 216–259 (2010).
27. Deshpande, A. P., Murali Krishnan, J. & Kumar, S. *Rheology of Complex Fluids* (Springer, 2010).
28. Raikher, Y. L., Rusakov, V. V. & Perzynski, R. Brownian motion in a viscoelastic medium modelled by a Jeffreys fluid. *Soft Matter* **9**, 10857–10865 (2013).
29. Yan, W. & Brady, J. F. The swim force as a body force. *Soft Matter* **11**, 6235–6244 (2015).
30. Ke, H. B., Zeng, J. F., Liu, C. T. & Yang, Y. Structure heterogeneity in metallic glass: modeling and experiment. *J. Mater. Sci. Technol.* **30**, 560–565 (2014).
31. Jiang, H.-R., Yoshinaga, N. & Sano, M. Active motion of a Janus particle by self-thermophoresis in a defocused laser beam. *Phys. Rev. Lett.* **105**, 268302 (2010).
32. Yan, J. et al. Reconfiguring active particles by electrostatic imbalance. *Nat. Mater.* **15**, 1095–1099 (2016).
33. Fuller, G. G. & Vermant, J. Complex fluid–fluid interfaces: rheology and structure. *Annu. Rev. Chem. Biomol. Eng.* **3**, 519–543 (2012).
34. Angelini, T. E. et al. Glass-like dynamics of collective cell migration. *Proc. Natl Acad. Sci. USA* **108**, 4714–4719 (2011).
35. Ni, R., Cohen Stuart, M. A. & Dijkstra, M. Pushing the glass transition towards random close packing using self-propelled hard spheres. *Nat. Commun.* **4**, 2704 (2013).
36. Berthier, L. Nonequilibrium glassy dynamics of self-propelled hard disks. *Phys. Rev. Lett.* **112**, 220602 (2014).
37. Stenhammar, J., Wittkowski, R., Marenduzzo, D. & Cates, M. E. Activity-induced phase separation and self-assembly in mixtures of active and passive particles. *Phys. Rev. Lett.* **114**, 018301 (2015).
38. Ni, R., Cohen Stuart, M. A., Dijkstra, M. & Bolhuis, P. G. Crystallizing hard-sphere glasses by doping with active particles. *Soft Matter* **10**, 6609–6613 (2014).
39. Lauga, E. Propulsion in a viscoelastic fluid. *Phys. Fluids* **19**, 083104 (2007).
40. Bi, D. & Yang, X., Marchetti, M. C. & Manning, M. L. Motility-driven glass and jamming transitions in biological tissues. *Phys. Rev. X* **6**, 021011 (2016).
41. Verstraeten, N. et al. Living on a surface: swarming and biofilm formation. *Trends Microbiol.* **16**, 496–506 (2008).

Acknowledgements

The authors acknowledge helpful discussions with Th. Voigtmann, M. Fuchs, D. Levis and J. Berner. We thank H.-J. Kümmerer and C. Mayer for their technical support. C.B. acknowledges financial support from the German Research Foundation (DFG) through the priority programme SPP 1726 on microswimmers and by the ERC Advanced Grant ASCIR (grant no. 693683). J.R.G.-S. was supported by DFG grant no. GO 2797/1-1.

Author contributions

C.L. and C.B. designed the research and wrote the paper; C.L. carried out the experiments and analysed the data; J.R.G.-S. performed the simulations.

Competing interests

The authors declare no competing interests.

Methods

Experimental details. The experiments were performed using a 50:50 binary mixture of small and large spherical silica particles. In our experiments, we used two different systems: mixtures with diameters $\sigma_S = 4.4 \pm 0.2\,\mu m$ and $\sigma_L = 6.3 \pm 0.2\,\mu m$ and mixtures with $\sigma_S = 1.8 \pm 0.2\,\mu m$ and $\sigma_L = 2.2 \pm 0.2\,\mu m$. In both cases, the size ratio, $\sigma_S/\sigma_L = 1.4$, suppresses crystallization and evolves glassy dynamics. As active particles, we used silica spheres with $\sigma = 6.3\,\mu m$ coated by a 30 nm thick layer of carbon on one hemisphere by thermal flash evaporation. All the particles (active and passive) were suspended in a mixture of water–2,6-lutidine (lutidine mass fraction 0.286), which exhibits a lower critical point at $T_c = 34\,°C$. The entire sample was kept below T_c at $T_0 = 26\,°C$. Under these conditions, the viscosity of the water–2,6-lutidine mixture was $\eta_\infty = 0.015 = Pa\,s$. On laser illumination, the solvent locally demixes at the heated carbon caps, which then leads to a self-propulsion opposite to the cap[21]. The rotational dynamics of active particles in the binary mixture and for $\varphi = 0$ is independent of the propulsion velocity entirely determined by the Brownian diffusion coefficient $D_\theta = k_B T/(\pi\sigma^3\eta)$, where η corresponds to the viscosity of the solvent[21,22].

The suspensions were loaded into a thin sample cell of height ~10 μm. To ensure a homogeneous particle density over the entire sample, the suspension was laterally confined (area 0.5 cm^2) by a structure of photoresist made by photolithography. All the sample cell surfaces were rendered negatively charged by a plasma treatment to avoid particle sticking.

To avoid ageing effects, data were collected at least 2 h after the sample was filled and sealed. The size of the region of interest was $62\sigma \times 50\sigma$. To avoid interactions with other APPs, we made sure that only a single active particle was within the field of view and adjacent regions. Video microscopy images were taken for at least 3,600 s at a rate of 10 fps using a charge-coupled device camera. From video images, particle positions $r = (x,y)$, spatial resolution ~50 nm and orientations $\boldsymbol{u} = (\cos\theta, \sin\theta)$ (the latter only applies to Janus particles) were obtained using Matlab image analysis software[21]. Area fractions were calculated as $\varphi = [n_S\pi(\sigma_S/2)^2 + n_L\pi(\sigma_L/2)^2]/A_I$, where n_S (n_L) is the number of small (large) particles in the field of view and A_T is the total area of the field of view, which results in a less than 1.5% error in φ.

Self-propulsion velocity. On illumination, APPs perform active motion (with the cap pointing opposite to the direction of motion, as is characteristic for polar particles) and their velocity v_0 depends on the incident light intensity I (Supplementary Fig. 2a). APP velocities v_0 for isolated particles ($\varphi = 0$) were determined from their short-time mean square displacements $\langle \Delta r\,(t)^2 \rangle = 4Dt + v_0^2 t^2$ (ref. [19]). When APPs are immersed in a dense colloidal suspension, their velocity strongly depends on the area fraction. Under such conditions, their velocity $v(\varphi)$ is obtained directly from the trajectories by calculating their displacement over time intervals of 2.5 s (Supplementary Fig. 2b). We confirmed that for time intervals between 0.5 and 10 s, only deviations below 10% in the velocity were obtained.

Glassy dynamics. In this subsection, we provide detailed information on the characterization of the glassy dynamics. As discussed in the main text, the global dynamics of the binary colloidal suspensions remains unaffected when adding a small amount of APPs. This is shown in Supplementary Fig. 1, where we plot $\langle \Delta r(t)^2 \rangle$ of a passive Janus particle for different area fractions. For $\varphi \le \varphi_g$, the motion at short times is subdiffusive due to collisions with the surrounding media. At later times, the Janus particle moves diffusively and the slope tends to 1. For $\varphi > \varphi_g$, the particle becomes trapped by its neighbours. This is in agreement with the typically observed slowing down due to caging[3,5]. Most importantly, the area fraction in which the plateau appears is identical to the glass transition of the passive binary mixture. This demonstrates that, for the propulsion velocities used in our study, the location of the glass transition is not changed by the presence of APPs. This is in contrast to dense disordered suspensions that entirely comprise active particles, for which a considerable shift of the glass transition is found[35,36].

In addition to the mean square displacements, we also measured the self-part of the intermediate scattering function[25] $F_s(\mathbf{q}, t) = \langle \exp\{-i\mathbf{q}\cdot[\mathbf{r}(t) - \mathbf{r}(0)]\}\rangle$ where $\mathbf{r}(t)$ is the position of a single particle at time t, and $\mathbf{q}$ is the scattering vector. In Supplementary Fig. 1b, we show F_s for $q = 6.95\,\mu m\,s^{-1}$ (which corresponds to the first peak of the structure factor at a high density). For the passive case, $v_0 = 0\,\mu m\,s^{-1}$ (solid symbols), F_s shows that the relaxation is fast and monoexponential at low φ. In the glass-forming phase, we observed the expected two-step relaxation behaviour; there was a clear intermediate plateau and the alpha relaxation occurred at increasingly longer timescales as φ increased. To confirm that the glassy structure was not affected by the activity, we also calculated F_s in the presence of APPs. The open symbols correspond to a passive particle located at more than 5σ from an APP (with $v_0 = 1.0\,\mu m\,s^{-1}$) during the measurement time. We found a good agreement in both cases. The structural relaxation time was obtained by fitting the final decay of F_s to a stretched exponential:

$$F_s(q,t) \sim \exp[-(t/\tau)^\beta] \tag{8}$$

where τ is the alpha relaxation time and the stretching exponent is typically $\beta \le 1$(Supplementary Fig. 4b). Our experimental data are well fitted by equation (8) in the range $0 < \varphi \le 0.776$ (solid lines).

Besides the extrapolations in Supplementary Fig. 1b, the existence of the glass phase was verified from the non-Gaussian parameter α_2, $\alpha_2(\Delta t) = \frac{\langle \Delta x^4 \rangle}{3\langle \Delta x^2 \rangle^2} - 1$ (Supplementary Fig. 1c). We see a clear indication of the approach to the glass transition in the rise of the peak value of α_2 as φ increases due to the cooperative out-of-cage displacements. Indeed, the peak rises and shifts towards longer times, which indicates a growing dynamic heterogeneity on approaching the glass transition. In contrast, the glass phase lacks cooperative out-of-cage motions, so α_2 exhibits no distinct peak and declines with time[3]. Such a sharp change has been regarded as a characteristic of a glass transition.

We found that at $\varphi_g > 0.776$, the self-diffusion coefficient, without and with activity, was ill-defined (Fig. 1f). Moreover, the relaxation time and the viscosity of the colloidal suspension extracted from the fit of the experimental data $\langle \Delta r(t)^2 \rangle$ (see below) diverges at $\varphi_g > 0.776$ (Supplementary Fig. 1b). It is noteworthy that the experiments performed with the same APP size immersed in a small passive binary mixture ($\sigma = 1.7$ and $2.4\,\mu m$) show the same tendency (Supplementary Fig. 3). We thus conclude that the glass transition is at $\varphi_g = 0.776$. This value is in agreement with the literature values[3].

Numerical mechanical model. Here we explain in detail the proposed model for the active motion of the APP through the colloidal background taking into account the coupling between translation and rotation as well as thermal fluctuations from the liquid solvent. In such a case, the mechanical response of the medium is delayed in time with respect to the particle velocity[27,28] (Fig. 3). Accordingly, as the APP motion is overdamped, the total force acting on it when moving at propulsion velocity v is:

$$\begin{aligned} 0 = &-\int_{-\infty}^{t} \zeta_{TT}(t-t')\,[\dot{\mathbf{r}}(t') - \mathbf{v}(t')]\,dt' \\ &-\int_{-\infty}^{t} \zeta_{TR}(t-t')\boldsymbol{\Omega}(t')\,dt' + \mathbf{F}^B \end{aligned} \tag{9}$$

where $\dot{\mathbf{r}}$ and $\boldsymbol{\Omega}$ are the translational and rotational velocities of the APP, v is the self-propulsive speed in the direction of the unit vector $\hat{\mathbf{u}}$, that is, $\mathbf{v}(t) = v\mathbf{u}(t)$. $\mathbf{F}^B$ is a zero mean random force with autocorrelation $\langle F_i^B(t) F_j^B(t') \rangle = k_B T \delta_{ij} \Gamma(t-t')$, which mimics thermal fluctuations. The term ζ_{TT} represents the force-translation coupling, whereas ζ_{TR} corresponds to the force-rotation coupling. According to our experimental observations, at $v = 0$ the translational drag is isotropic $\zeta_{TT}(t-t') = \mathbf{I}\Gamma(t-t')$, where $\mathbf{I}$ is the isotropic tensor and $\Gamma(t) = 3\pi\sigma G_\varphi(t)$ with G_φ being the corresponding stress-relaxation modulus. Moreover, the translation-rotation coupling term vanishes on average, as the APP does not exhibit a persistent rotation $\langle \Omega = 0 \rangle$. Therefore, it behaves as a noise term in addition to the thermal noise $\mathbf{F}^B$. Consequently, we can write the Langevin equation for the 2D translational motion of the APP as:

$$0 = \mathbf{F}_{TT}(t) + \boldsymbol{\xi}(t) \tag{10}$$

where

$$\mathbf{F}_{TT}(t) = -\int_{-\infty}^{t} \Gamma(t-t')\,[\dot{\mathbf{r}}(t') - v\mathbf{u}(t')]\,dt' \tag{11}$$

is the total force due to the force-translation coupling, whereas:

$$\boldsymbol{\xi}(t) = -\int_{-\infty}^{t} \zeta_{TR}(t-t')\boldsymbol{\Omega}(t')\,dt' + \mathbf{F}^B \tag{12}$$

Note that the total force exerted by the surrounding medium on the particle vanishes on average, $\langle F_{TT}(t) \rangle = -\langle \xi(t) \rangle = 0$, and thereby fulfils the force-free condition in the absence of external forces. However, similar to active Brownian motion models for self-propulsion in purely viscous liquids, the term:

$$\mathbf{F}_{prop}(t) = -v\int_{-\infty}^{t} \Gamma(t-t')\mathbf{u}(t')\,dt' \tag{13}$$

in equation (11) can be interpreted as is an internal force[29] that describes the propulsion of the APP with velocity v. Therefore, due to the memory kernel, the drag force is

$$\mathbf{F}_{drag}(t) = -v\int_{-\infty}^{t} \Gamma(t-t')\mathbf{u}(t')\,dt' - \boldsymbol{\xi}(t) \tag{14}$$

Importantly, apart from small deviations due to thermal noise, the drag force $\mathbf{F}_{drag}(t)$ is antiparallel to $\mathbf{F}_{prop}(t)$, but not to the particle orientation $\mathbf{u}(t)$ which depends on all previous times. Note that this time delay can be regarded as a rotational–translational coupling that leads to an effective torque on the particle. Owing to the symmetry of the APP with respect to its orientation, we introduce an effective lever arm $\mathbf{L} = \mu\sigma\mathbf{u}(t)$, which is defined relative to the particle centre (Fig. 4b). Thus, we model the rotational–translational coupling as a time-dependent torque:

$$\mathbf{T}(t) = \mu\sigma\mathbf{u}(t) \times \mathbf{F}_{drag}(t) \tag{15}$$

As the size of L depends on the local asymmetry in the structure of the surrounding medium, it is considered as a free fitting parameter μ. However, we observed experimentally that the rotational dynamics takes place in 2D. Therefore, the equation of motion of the APP orientation reads:

$$\frac{\mathrm{d}\mathbf{u}}{\mathrm{d}t} = \boldsymbol{\Omega} \times \mathbf{u} \rightarrow \frac{\mathrm{d}\theta}{\mathrm{d}t} = \boldsymbol{\Omega} \tag{16}$$

In contrast to the translational motion, the mean-square angular displacement $\langle \Delta\theta(t)^2 \rangle$ of the APP at $v = 0$ is purely diffusive for all area fractions (Fig. 2b), which implies no memory for the orientational motion. Accordingly, the evolution of θ can be modelled by the Markovian Langevin equation:

$$\pi\sigma^3\eta_\theta\dot{\boldsymbol{\theta}}(t) + \boldsymbol{\xi}_\theta(t) + \mathbf{T}(t) = 0 \tag{17}$$

where η_θ is the rotational viscosity (extracted from the slope of the $\langle \Delta\theta(t)^2 \rangle$) (Fig. 2b). Here, $\boldsymbol{\xi}_\theta(t)$ is a Gaussian noise of zero mean and $\xi_\theta(t)\xi_\theta(t') = 2k_\mathrm{B}T\pi\sigma^3\eta_\theta\,\delta(t-t')$, which mimics thermal fluctuations. In combination with the noise, the presence of a time-dependent torque leads to an enhanced rotational diffusion coefficient, as observed in our experiments.

To numerically solve the angular equation of motion of the APP, equation (5), the parameters that describe the rheological properties of the binary colloidal suspension, that is, η_∞, η_θ, η_0, τ, τ_{SLS} and g_2 have to be determined experimentally. The viscosity of the water–lutidine solvent, η_∞, was obtained from the 2D translational mean-square-displacement, $\langle \Delta r(t)^2 \rangle = 4Dt$ of an isolated passive particle ($v_0 = 0\,\mu\mathrm{m\,s^{-1}}$) by means of the Stokes–Einstein relation, $\eta_\infty = k_\mathrm{B}T/(3\pi\sigma D)$. The value of η_θ is given by $\eta_\theta = k_\mathrm{B}T/(\pi\sigma^3 D_\theta)$, where $D_\theta = 0.0011 \pm 5\times10^{-5}\,\mathrm{s^{-1}}$ is obtained from Fig. 2b. The other parameters, which strongly depend on φ, are obtained by fitting the experimental $\langle \Delta r(t)^2 \rangle$ of a passive colloid to that obtained from the Langevin model given by equation (3). For this purpose, we set $v = 0$ in equation (3) and Fourier transformed to obtain analytical expressions of $\langle \Delta r(t) \rangle$ for the two different mechanical models below and above the glass transition. For $\varphi < \varphi_\mathrm{g}$, using equation (6) for the viscoelastic fluid model:

$$\langle |\boldsymbol{\Delta} r(t)^2| \rangle = \frac{4k_\mathrm{B}T}{3\pi\sigma\eta_0}\left\{ t + \frac{\eta_0 - \eta_\infty}{\eta_0}\tau\left[1 - \exp\left(-\frac{\eta_0}{\eta_\infty\tau}t \right) \right] \right\} \tag{18}$$

from which we get η_0 and τ, whereas $\varphi > \varphi_g$, equation (7), yields:

$$\langle |\boldsymbol{\Delta} r(t)^2| \rangle = \frac{4k_\mathrm{B}T}{3\pi g_2}\frac{g_1}{g_1 + g_2}\left[1 - \exp\left(-\frac{g_1}{g_1 + g_2}t \right) \right] \tag{19}$$

which allows us to extract τ_{SLS} and g_2.

This is illustrated in Supplementary Fig. 4a, in which we plot some examples of such fits of the experimental data to equation (18) for area fractions below the glassy state ($\varphi = 0.453$ and 0.776), and to equation (19) at $\varphi = 0.814 > \varphi_g$. Using the fitted experimental data in Supplementary Fig. 4b,c, we show the divergence of the viscosity η_0 and τ at φ_g, respectively, and the elastic moduli

The propulsion velocity of an APP is strongly affected by the viscoelastic colloidal surrounding. To determine such values for the numerical simulations, we note that the motion of an isolated APP in a pure solvent ($\varphi = 0$) at v_0 results from a propulsion force $3\pi\eta_\infty\sigma v_0$. With $\varphi < \varphi_\mathrm{g}$, for the APP to move with the same force, its propulsion speed v must satisfy:

$$v\int_{t_0}^{t} \Gamma(t-t')\,\mathrm{d}t' = 3\pi\eta_\infty\sigma v_0 \tag{20}$$

and using the expression of the memory kernel for the viscoelastic liquid, we obtain

$$v = (\eta_\infty/\eta_0)\,v_0 \tag{21}$$

which implies that $v < v_0$. For $\varphi > \varphi_g$, the viscous forces on the APP are only due to the solvent viscosity η_∞. In such a case, due to the dynamical arrest, the total force exerted by the surrounding medium on the APP is on average zero. Thus, the propulsion force is balanced by the restoring force exerted by the purely elastic component (modulus $g_1(\varphi)$), which leads to $v = v_0$ Note that a simple Maxwell model[27] for the case $\varphi > \varphi_g$, that is, $\eta_\infty = 0$ in equation (6) or $g_2 = 0$ in equation (7), is not enough to describe the minimal features of our system. In such a case, a straightforward calculation leads to a purely diffusive mean-square displacement (equation (19)), in disagreement with our experimental observations. Indeed, the SLS model has a mechanical relaxation time $\tau_{\mathrm{SLS}}(\varphi) = \frac{\eta_\infty}{g_1(\varphi)}$, which is much smaller than the hopping time[5]. Therefore, the proposed model should work well for almost fully arrested regimes.

Enhanced dynamics for colloidal backgrounds that comprised smaller particles. To support the robustness of the observed features, we also studied the dynamics of an embedded APP of diameter 6.3 µm for other particle size ratios of the binary colloidal suspension with $\sigma_\mathrm{S} = 1.8\,\mu\mathrm{m}$ and $\sigma_\mathrm{L} = 2.2\,\mu\mathrm{m}$. In Supplementary Fig. 3, we show the corresponding relaxation time (Supplementary Fig. 3a), effective translational diffusion and normalized rotational diffusion coefficient. The minimal model, equation (5), also reproduces the enhanced D_θ^{APP}. In this case, the best agreement with our experimental data is obtained for $\mu = 0.20$ for $\varphi < \varphi_\mathrm{g}$ and $\mu = 0.78$ for $\varphi > \varphi_\mathrm{g}$, respectively. The occurrence of enhanced dynamics in other crowded environments also suggests the effect to be generic for viscoelastic suspensions with large structural relaxation times. The increased enhancement of D_θ^{APP} for smaller background particles can be understood by the larger number of contacts between the probe and the background, which leads to a stronger coupling[12].

Fluctuations of the angle between particle velocity and its orientation. The effect of the time-delayed response of a viscoelastic environment on the misalignment between $\mathbf{u}(t)$ and $\dot{\mathbf{r}}$ is quantified by means of the s.d. of the α distribution. Supplementary Fig. 5 shows the results obtained for different area fractions and different self-propulsion velocities. Interestingly, the global behaviour obtained can be easily related to that reported in Fig. 2c for the enhancement of D_θ^{APP}. On increasing φ, the fluctuations of the particle orientation relative to its direction of motion increase in a manner very similar to the behaviour of the rotational diffusion coefficient.